Mechano-chemical feedback leads to competition for BMP signalling during pattern formation

Daniel J. Toddie-Moore[1¶*], Martti P. Montanari[1#], Ngan Vi Tran[2#], Evgeniy M. Brik[2], Hanna Antson[2], Isaac Salazar-Ciudad[1,3,4] and Osamu Shimmi[1,2*]

[1]Institute of Biotechnology, University of Helsinki, 00014 Helsinki, Finland

[2]Institute of Molecular and Cell Biology, University of Tartu, 51010 Tartu, Estonia

[3]Genomics, Bioinformatics and Evolution. Departament de Genètica i Microbiologia, Universitat Autònoma de Barcelona, 08193, Cerdanyola del Vallès, Spain

[4]Centre de Rercerca Matemàtica, 08193, Cerdanyola del Vallès, Spain

[*]Corresponding authors: d.toddie-moore@ed.ac.uk and osamu.shimmi@helsinki.fi

[¶]Present address: Wellcome Centre for Cell Biology, School of Biological Sciences, University of Edinburgh, Edinburgh, UK.

[#]M.P.M. and N.V.T. contributed equally to this work.

Abstract

Developmental patterning is thought to be regulated by conserved signalling pathways. Initial patterns are often broad before refining to only those cells that commit to a particular fate. However, the mechanisms by which pattern refinement takes place remain to be addressed. Using the posterior crossvein (PCV) of the *Drosophila* pupal wing as a model, into which bone morphogenetic protein (BMP) ligand is extracellularly transported to instruct vein patterning, we investigate how pattern refinement is regulated. We found that BMP signalling induces apical enrichment of Myosin II in developing crossvein cells to regulate apical constriction. Live imaging of cellular behaviour indicates that changes in cell shape are dynamic and transient, only being maintained in those cells that retain vein fate after refinement. Disrupting cell shape changes throughout the PCV inhibits pattern refinement. In contrast, disrupting cell shape in only a subset of vein cells can result in a loss of BMP signalling. In addition, we observed that expressing the constitutively active form of the BMP type I receptor in clones caused apical constriction autonomously and often induced BMP signalling loss in the PCV region in a non-autonomous manner. We propose that the cell shape changes of future PCV cells allow them to compete more efficiently for the basally localised BMP signal by forming a mechano-chemical feedback loop. This study highlights a new form of competition among the cells: competing for a signal that induces cell fate.

Introduction

Pattern formation is a fundamental process in animal development, for which various molecular mechanisms have been proposed, including gene regulatory networks and growth factor signalling[1,2]. Developmental patterning often involves refinement from a broad initial area of competency for a fate to only those cells that commit to it, with neighbours losing competence and following an alternate fate path (Fig. 1a)[1,2]. Whilst some mechanisms of pattern refinement, such as

43 transcriptional networks and lateral inhibition, have previously been investigated, the role played by
44 diffusible growth factor signalling, in particular the interactions between signalling and
45 morphogenesis, has been less explored[3,4].
46 The posterior crossvein (PCV) of the *Drosophila* pupal wing serves as an excellent model to
47 address the dynamics of signalling and morphogenesis, as its formation is initially directed by a
48 single signalling pathway: Bone morphogenetic protein (BMP) signalling[5,6]. The *Drosophila* BMP
49 ligand Decapentaplegic (Dpp) is initially expressed in the adjacent longitudinal veins (LVs) and is
50 extracellularly transported into the prospective PCV region along the basal surfaces of the two cell
51 layers that comprise the wing epithelia (Fig. 1b)[7]. Extracellular transport at this stage requires the
52 BMP binding proteins Short gastrulation (Sog) and Crossveinless (Cv) which bind to the Dpp
53 ligand and facilitate its active transport into the PCV region[8,9].
54 BMP signalling induced by the Dpp ligand forms the PCV field, directing cells to become
55 competent for vein, rather than the intervein fate that occurs if BMP signalling is not activated or is
56 not sustained (Fig. 1c)[5,8]. Continuous extracellular Dpp transport seems to be crucial for a period of
57 around 10 hours (18 – 28 h after pupariation (AP)) to maintain the PCV field and vein fate
58 competence, before PCV cells begin to express the ligand themselves[5]. Continued extracellular
59 signalling and vein morphogenesis occur concurrently, as morphogenesis begins shortly after BMP
60 signalling is activated[6]. Refinement of the BMP signalling pattern during this time window has
61 previously been observed; however, how pattern refinement takes place has not been addressed[10].
62 In this study, to understand how refinement of the BMP signalling takes place during PCV fate
63 determination, we utilised *Drosophila* genetics and *in vivo* live imaging. Our data reveal that the
64 dynamics of cell shape direct refinement by forming a mechano-chemical feedback loop that drives
65 competition for the vein-fate-determining BMP signal.
66
67 **Results**

68 **BMP signalling induces cell shape changes during pattern refinement**

69 First, we confirmed that refinement of the PCV field takes place during PCV morphogenesis. The
70 PCV field is defined as the cells in which BMP signalling occurs, as indicated by staining with anti-
71 phosphorylated Mad antibody (pMad)[11], and which are therefore competent to assume a vein fate.
72 Our data reveal that the number of cells within the PCV field reduces between 20h AP, shortly after
73 the initiation of PCV patterning, and 28h AP, when PCV cells express *dpp* themselves (Fig. 1d, e).
74 Thus we term the period from 20 to 28 hours AP the 'refinement period'.

75 During this period, apical constriction of vein cells appears to be the hallmark of vein
76 morphogenesis[10,12,13]. Since BMP signalling is thought to initiate PCV development[7], we next asked
77 whether BMP signalling directs the wing vein-like cell shape changes (hereafter referred to as "cell
78 shape changes") that occur during PCV morphogenesis. To answer this question, we captured
79 images of apical cell shapes in the PCV region of *crossveinless* mutant wings, into which Dpp
80 cannot be transported, and where BMP signalling is thus inactive. We observed that apical
81 constriction does not occur where the PCV normally forms (Fig. 1f)[8], indicating that BMP
82 signalling is required for the cell shape changes that occur during PCV morphogenesis.

83 The activity of Myosin II (MyoII) has been proposed to be the driving force behind cell shape
84 dynamics such as apical constriction[14]. To investigate whether BMP signalling directs cell shape
85 change through MyoII activity, we analysed the spatial localisation of MyoII using MyoII
86 regulatory light chain (MRLC) tagged with RFP in wild type and *crossveinless* pupal wings[15]. In
87 wild type wings, MyoII is enriched in the apical compartment of PCV cells, with lower basal levels,
88 but in contrast, neighbouring intervein cells have lower apical levels of MyoII than the PCV (Fig.
89 1g, Supplementary Fig. 1a). Conversely, in *crossveinless* pupal wings, apical MyoII enrichment is
90 not observed in the PCV region, although apical enrichment of MyoII is still detected in LVs (Fig.
91 1g, Supplementary Fig. 1a). These findings suggest that BMP signalling facilitates the apical
92 localisation of MyoII to promote apical constriction of PCV cells. This was further confirmed by

93 the observation that ectopic expression of the constitutively active form of BMP type I receptor
94 Thickveins (Tkv^{QD}) in mosaic analysis with a repressible cell marker (MARCM) clones within the
95 pupal wing induces apical enrichment of MyoII and apical constriction (Supplementary Fig. 1b)[10,16].

96 **Time lapse imaging during PCV morphogenesis reveals reversible fate path**

97 As wing vein morphogenesis directed by BMP signalling and refinement of the BMP signalling
98 pattern occur concurrently, we hypothesised that these events could be mutually coordinated. To
99 address this, we employed *in vivo* live imaging of pupal wings expressing GFP-tagged E-cadherin
100 (E-cad::GFP) to observe cell shape changes during the refinement period[17]. We tracked the apical
101 shapes of cells that are part of the PCV at the end of the refinement period, and thus retained vein
102 fate competence, and compared them to the cells flanking this region (Fig. 2a-c, Supplementary
103 Videos 1-3). Intriguingly, whilst the cells that will form the PCV constrict apically throughout the
104 refinement period, several of the cells immediately flanking these constrict apically at early time
105 points, but fail to maintain their vein-like morphology at later time points, eventually reverting to an
106 intervein fate (Fig. 2a-d, Supplementary Videos 1, 2).

107 **Cell shape change and pattern refinement are coupled**

108 We hypothesised that cell shape changes themselves may affect signalling pattern refinement and
109 thus cell fate choice in the PCV region. To test this idea, we modulated cell shape changes in the
110 developing wing by attenuating MyoII activity using a dominant negative form of the Myosin
111 Heavy Chain (MyoII-DN)[18]. Inhibiting MyoII activity across the posterior wing blade for 10 hours
112 during PCV morphogenesis is sufficient to disrupt apical constriction in the PCV region and LV
113 cells of 23h AP pupal wings (Fig. 3a-c). Intriguingly, loss of MyoII activity throughout the
114 posterior wing results in a broader range of BMP signalling in the PCV region than in control
115 wings, suggesting that cell shape changes are necessary for the refinement of the BMP signalling,
116 but not for BMP signalling itself (Fig. 3d, e). Consistently, adult wings show disrupted PCV
117 patterning, manifesting both as vein thickenings and branches that extend from the normally straight

118 PCV, suggesting that the organisation of cell fates has been disrupted (Fig. 3f). Additionally, BMP
119 signalling was missing in the PCV region when MyoII activity was disrupted in the posterior half of
120 *crossveinless* wings, indicating that the unrefined BMP signalling pattern is still being directed by
121 extracellular BMP signalling (Supplementary Fig. 2a). We further confirmed that dynamic MyoII
122 activity is crucial for refinement of BMP signalling using the ectopic expression of constitutively
123 active Myosin binding subunit (Mbs), a regulatory subunit of myosin phosphatase, which also leads
124 to a broader range of BMP signalling in the PCV region (Supplementary Fig. 2b, c)[19].
125 What then is the role of cell shape changes in signalling pattern refinement? Despite reversal of
126 BMP-induced cell shape changes being associated with reduced competence for vein fate, blocking
127 cell shape changes did not affect BMP signalling. We hypothesised that what might be important is
128 not cell shape change itself, but how cell morphology compares to that of other cells within the
129 field. The impact of cell shape change loss may then be context-specific, facilitating refinement by
130 causing less signalling and subsequent fate loss in cells surrounded by those with greater changes in
131 shape. If this is the case, inhibition of cell shape changes in a small group of cells within the PCV
132 field may decrease their ability to retain BMP signalling and vein fate. We tested this hypothesis by
133 generating clones that attenuate cell shape changes amongst neighbours that are wild type.
134 Strikingly, when MyoII-attenuated clones are produced within the PCV field, loss of BMP
135 signalling can often be observed in a context-dependent manner (Fig. 3g, Supplementary Fig. 2d, e).
136 This suggests that MyoII-based cell shape changes play a crucial role in whether a cell retains vein
137 fate during refinement, despite these shape changes not being required for BMP signalling. When
138 all PCV field cells cannot form vein-like shapes, signalling still occurs throughout, and refinement
139 does not take place (Fig. 3a-e, h). However, when cells are present in a heterogeneous population
140 with or without cell shape changes, cells that can change shape both retain the signal and acquire
141 vein fate (Fig. 3g, h). We propose that cells of the PCV field may be competing for BMP signalling
142 via their changes in cell shape, with those that can change and retain vein-like shapes being more

143 readily able to retain BMP signalling than their neighbours. Furthermore, our data indicate that the
144 mechanism of pattern refinement is a self-organising mechano-chemical feedback loop, as BMP
145 signalling induces the cell shape changes, which in turn influence the ability of cells to retain that
146 signal.

147 **Competition for BMP signalling takes place at the PCV region**

148 As BMP signalling appears to be needed for the refinement of the signal itself, we hypothesise that
149 stronger signalling may make the cells more competitive for receiving the signal. Therefore, we
150 generated strongly apically constricting clones expressing the constitutive active form of the BMP
151 type I receptor (Tkv^{QD}) and examined whether they perturbed endogenous BMP signalling at the
152 PCV. Strikingly, wings carrying tkv^{QD} clones often lose pMad signal in the PCV region, but not in
153 LVs (Fig. 3i), suggesting that cells expressing Tkv^{QD} become super competitive for BMP signalling
154 in a non-autonomous manner. This strongly supports the hypothesis that cells compete for BMP
155 signalling in the PCV field, and that high levels of signalling in some cells are able to perturb
156 signalling in others.

157 How do clones of ectopic BMP signalling non-cell-autonomously affect the ability of PCV region
158 cells to receive the BMP signal? It is tempting to propose that they may capture extracellular Dpp
159 ligand more readily, allowing them to out-compete others for the BMP signal. To address this, we
160 generated clone cells expressing Tkv^{QD}, but with less ability to capture the Dpp ligand. Since
161 previous studies suggested that dynamin-mediated endocytosis plays a crucial role in BMP
162 signalling and Dpp ligand capture in the wing imaginal disc[20], we first tested whether this was also
163 the case in the pupal wing. When clone cells of temperature-sensitive dynamin mutant ($shibire^{ts1}$;
164 shi^{ts1}) are generated in the PCV region, pMad signal is often lost autonomously (Supplementary
165 Fig. 3a), indicating that dynamin-mediated endocytosis is crucial for BMP signalling during PCV
166 development. Next, we generated shi^{ts1} clones co-expressing tkv^{QD}. Although BMP signalling in
167 these clones is still robust, BMP signalling in the PCV region is no longer disrupted (Fig. 3j). Taken

168 together this indicates that cells with strong BMP signalling can outcompete other cells at the level
169 of ligand capture through cell shape changes, decreasing their neighbours' signalling capabilities.

170 **Basal cell shape changes facilitate competition between cells and pattern refinement**

171 We next considered what the mechanism of competition between cells for the BMP signal is, and
172 how cell shape might play a role. Previous studies indicate that extracellularly trafficked Dpp
173 ligands are predominantly localised on the basal side of the wing epithelia[7], therefore, the basal side
174 of PCV field cells can be considered as the signalling micro-environment. We hypothesized that
175 apical constriction may cause an expansion in basal cell size that could increase competence for
176 capturing basally localised ligand. To investigate this, we compared the apical and basal cell sizes
177 of cells both within and outside of the PCV field during the refinement period (Fig. 4a). We observe
178 that as cells within the PCV field (BMP signal positive) apically constrict, they also basally expand,
179 unlike cells outside of the PCV field (BMP signal negative) (Fig. 4b-d). Since the volume of cells is
180 largely conserved throughout the refinement period (Supplemental Fig. 4a), it appears that basal
181 expansion is induced by BMP-induced apical Myosin II without changing cell volume.

182 We next investigated whether there was any difference in basal cell size between cells at the
183 periphery of the PCV field, which may shortly lose vein fate competence, and the centre of the PCV
184 field (Fig. 4e). We found that cells at the periphery often had smaller basal surfaces than those at the
185 centre between 22 and 26 h AP, suggesting that cells which are to shortly lose their vein fate are
186 less basally expanded (Fig. 4f-h).

187 To examine whether differential basal cell size is a mechanism by which cells could compete for the
188 BMP signal, we observed whether differences in basal cell size within the PCV field are still
189 observed when refinement does not take place due to attenuated MyoII activity. Our data reveal
190 that, compared to wild type wings, there are much less pronounced differences in basal cell size
191 between central and peripheral cells when MyoII is disrupted in the posterior half of pupal wing

192 (Supplementary Fig 4b, c). These observations are consistent with basal cell size dynamics playing
193 a role in the mechanism of refinement.
194 We next sought to ask how these changes in cell shape could make cells more competent for the
195 BMP signal. A larger basal surface would allow a cell to occupy more space in the signalling
196 microenvironment, however whether this would allow a cell to signal more would depend on how
197 this impacted upon its ability to display the appropriate receptors. We investigated Tkv expression
198 during PCV refinement, and found that Tkv localization is observed at the basal compartment in
199 BMP positive cells, but not in negative cells (Fig. 5a, Supplementary Fig. 5a), suggesting that the
200 cellular compartmentalisation of Tkv is regulated through a positive feedback mechanism.
201 Correspondingly, Dpp ligands accumulate at the basal compartment in the PCV field during the
202 refinement period (Supplementary Fig. 5b). Next, we quantified the interactions between basal cell
203 area and integrated density of basally localized Tkv in the PCV field. Our data reveal that larger
204 basal surface areas in PCV field cells correlated with higher overall intensities of Tkv, and that
205 lower intensities of Tkv were observed for peripheral cells (Fig. 5b). Taken together, these results
206 suggest that the mechanism by which vein-like cell shape changes facilitates cells to compete for
207 the BMP signal is by promoting higher receptor localisation on the basal surface.
208
209 **Discussion**
210 Here we found that cell shape changes are coupled to the refinement of BMP signalling during PCV
211 morphogenesis. Our findings reveal that the formation of a mechano-chemical feedback loop drive
212 competition for the vein fate-determining BMP ligand, with less competitive cells acquiring
213 intervein cell fate. Therefore, different competence for the BMP signal leads to differential cell fate
214 determination (vein or intervein) in later pupal development (Fig. 6a). Our data provide the
215 evidence that clones of super competent cells are generated by expression of Tkv^{QD} (Fig. 3i) and
216 that these can outcompete surrounding wild type cells and cause BMP signalling in the PCV field to

217 be lost in a non-cell autonomous manner. The mechanism by which Tkv^{QD} clone cells dominate the
218 BMP signal in the PCV field is not fully understood, however, Tkv^{QD} clone cells in *shi* mutants do
219 not show such super competence (Fig. 3j), suggesting that high BMP signalling alone is not
220 sufficient to increase competence. Converse results derived from context-specific expression of
221 MyoII-DN provide further insights (Fig. 3). Basal cell shape changes via BMP signal-induced
222 apical MyoII appear to be important for the determination of BMP positive and negative cells
223 through generating differences among cells within the field, and may allow cells to compete for the
224 extracellular ligand more efficiently. We propose that BMP signal-induced cell shape changes (via
225 apical MyoII) provide the molecular mechanisms to increase competence for the BMP signal by
226 forming a mechano-chemical feedback loop (Fig. 6b).
227 We propose that cells in the PCV field are in competition to receive the BMP signal during the
228 refinement period. Our data suggest that basal surface dynamics form part of the mechanism of
229 competition for the signal for the following reasons. First, the basal surface areas of PCV progenitor
230 cells expand during the refinement period in a BMP dependent manner (Fig. 4). Second, basal
231 surface sizes of peripheral PCV cells are significantly smaller than those at the centre of the PCV
232 region (Fig. 4g, h). Third, Tkv sufficiently localizes at the basal compartment in the PCV region to
233 capture basally trafficked Dpp ligand, and is present in greater quantities in basally expanded cells
234 (Fig. 5, Supplementary Fig. 5). It is possible that cell shape changes play a role in promoting basal
235 Tkv localisation, for example by downward cytoplasmic flow. Fourth, less significant differences of
236 basal surface areas between the cells in the PCV region are noted when MyoII activity is disrupted
237 (Supplementary Fig. 4b, c). Taken together, our observations indicate that BMP-induced apical
238 MyoII leads to basal expansion, resulting into increasing competence for the BMP signal (Fig. 6).
239 Previous studies have proposed that competition between cells for BMP signalling instructs the
240 pattern of survival and elimination in the Drosophila wing imaginal disc[21-23]. Since BMP signalling
241 is one of the key players regulating cell proliferation in the larval wing imaginal disc[24,25], cells

242 lacking BMP signalling are less proliferative than neighbouring cells and are eliminated as loser
243 cells[26]. Although BMP still serves as a proliferative signal in the *Drosophila* wing during the early
244 pupal stage[27,28], BMP turns into a cell differentiation factor at the beginning of the refinement
245 period and thus competition for it has a different outcome. However, unlike in classical cell
246 competition, acquiring more Dpp ligand does not confer a selective advantage for survival, rather an
247 alternative fate path (vein or intervein).
248 Unlike our recent observations that the 3D architecture of pupal wing epithelia (comprising of two
249 apposing epithelial cell layers) and BMP signalling in the LVs are coupled[29], PCV refinement
250 appears to be a 2D phenomenon, as large single-layer clones expressing MyoII-DN that disrupt 3D
251 architecture have been observed that do not affect refinement in the other layer (Supplementary Fig.
252 2e). This finding is intriguing, as we previously described that single-layer mutant clones of the
253 Rho-GAP crossveinless-C (CV-C), which promotes Dpp ligand transport, could affect BMP
254 signalling in the PCV region of the other layer[6]. These phenomena are likely to be distinct, as unlike
255 when expressing MyoII-DN, small clones of *cv-c* mutants do not lose BMP signalling, whereas
256 larger ones do. These results suggest that the inter-layer effects previously observed for *cv-c* mutant
257 clones require the proper apposition of the two wing layers, which is locally disrupted in both
258 MyoII-DN clones and tissue-level MyoII-DN expression (Supplementary Fig. 4d).
259 How cell shape-based competition for Dpp ligand allows refinement to form a neat stripe of vein
260 cells is still not clear. We postulate that cells surrounded by other BMP-positive apically constricted
261 cells will be more readily able to form a vein-like shape themselves, a phenomenon likely to be
262 amplified by the mechanical feed-forward loop we have identified. This could explain why cells at
263 the edge of the field, next to intervein cells, are less able to expand basally, and thus are more likely
264 to lose BMP signalling competence, leaving a stripe of vein-fated cells. Non-cell autonomous feed-
265 forward factors downstream of BMP signalling, such as Cv-C, could also play a role, as optimising
266 the extracellular transport of Dpp affects not only an individual cell but also other cells nearby. It is

267 tempting to speculate whether differences in signalling induced by differential cell shape changes
268 can play a role in the refinement of the extracellular ligand range, reinforcing differences in cell
269 shape. Notably, not all peripheral cells are smaller than all central cells at any one snapshot (Fig.
270 4g). This is consistent with the PCV field not refining uniformly, with different sides or positions
271 within the field refining at different times (Fig. 2c). However, it could also be the case that smaller
272 central cells are able to persist because of an accommodating environment generated by basally
273 expanded cells nearby.
274 We hypothesize that cell shape-based competition for an extracellular signalling component is
275 likely to be a general mechanism for self-organisation of pattern refinement during development.
276 Cell shape changes are a common part of the morphogenesis programme and could feed back into
277 developmental patterning in a variety of contexts[3,4]. Apical constriction and basal expansion are an
278 important aspect of epithelial folding, a process which has broadly been linked to cell fate decisions
279 and developmental patterning[3,4,30,31]. Our finding that cell shape changes within the 2D epithelial
280 layer, irrespective of epithelial folding, can instruct pattern refinement provides a novel insight into
281 epithelial morphogenesis.
282 In summary, our data reveal that cell shape changes influence refinement of the signalling pattern
283 by facilitating cells to compete for signalling pathway activation. We have uncovered that
284 competition for extracellular BMP ligand occurs via a mechano-chemical feedback loop between
285 cell shape changes and BMP signalling, leading to self-organising refinement of the developmental
286 field during pattern formation.
287

288 **Acknowledgements**

289 We are grateful to Jukka Jernvall, Charlotte Repton and Yukitaka Ishimoto for thoughtful
290 comments on the manuscript. We thank the Light Microscopy Unit of the Institute of Biotechnology
291 of the University of Helsinki for their support. We thank G. Pyrowolakis, H. Ohkura, R. Le Borgne,

D. Kiehart, T. Kornberg and A. Martin for fly stocks. This work was supported by grant 308045 from the Academy of Finland, the Sigrid Juselius Foundation to O.S., grant 295013 from the Academy of Finland to D.T-M., and the Center of Excellence in Experimental and Computational Developmental Biology from the Academy of Finland to O.S. and I.S-C.

Author contributions

D.T-M. and O.S. conceived the project and planned experiments. D.T-M., M.P.M., N.V.T. and H.A. performed experiments. D.T-M., M.P.M., N.V.T., E.M.B. and H.A. analysed the results and discussed them with O.S. I.S-C. provided inputs. D.T-M. and O.S. wrote the manuscript and all authors made comments. O.S. supervised the project.

Declaration of interests

The authors declare no competing interest.

Data availability

The datasets generated and analysed during the current study are available from the corresponding authors on reasonable request.

References

1 Schweisguth, F. & Corson, F. Self-Organization in Pattern Formation. *Dev Cell* **49**, 659-677, doi:10.1016/j.devcel.2019.05.019 (2019).

2 Morelli, L. G., Uriu, K., Ares, S. & Oates, A. C. Computational approaches to developmental patterning. *Science* **336**, 187-191, doi:10.1126/science.1215478 (2012).

3 Hannezo, E. & Heisenberg, C. P. Mechanochemical Feedback Loops in Development and Disease. *Cell* **178**, 12-25, doi:10.1016/j.cell.2019.05.052 (2019).

317 4 Gilmour, D., Rembold, M. & Leptin, M. From morphogen to morphogenesis and back.
318 *Nature* **541**, 311-320, doi:10.1038/nature21348 (2017).
319 5 Ralston, A. & Blair, S. S. Long-range Dpp signaling is regulated to restrict BMP signaling
320 to a crossvein competent zone. *Dev Biol* **280**, 187-200, doi:10.1016/j.ydbio.2005.01.018
321 (2005).
322 6 Matsuda, S., Blanco, J. & Shimmi, O. A feed-forward loop coupling extracellular BMP
323 transport and morphogenesis in Drosophila wing. *PLoS Genet* **9**, e1003403,
324 doi:10.1371/journal.pgen.1003403 (2013).
325 7 Matsuda, S. & Shimmi, O. Directional transport and active retention of Dpp/BMP create
326 wing vein patterns in Drosophila. *Dev Biol* **366**, 153-162, doi:10.1016/j.ydbio.2012.04.009
327 (2012).
328 8 Shimmi, O., Ralston, A., Blair, S. S. & O'Connor, M. B. The crossveinless gene encodes a
329 new member of the Twisted gastrulation family of BMP-binding proteins which, with Short
330 gastrulation, promotes BMP signaling in the crossveins of the Drosophila wing. *Dev Biol*
331 **282**, 70-83, doi:10.1016/j.ydbio.2005.02.029 (2005).
332 9 Shimmi, O. & Newfeld, S. J. New insights into extracellular and post-translational
333 regulation of TGF-beta family signalling pathways. *J Biochem* **154**, 11-19,
334 doi:10.1093/jb/mvt046 (2013).
335 10 Gui, J., Huang, Y. & Shimmi, O. Scribbled optimizes BMP signaling through its receptor
336 internalization to the Rab5 endosome and promote robust epithelial morphogenesis. *PLoS*
337 *Genet* (2016).
338 11 Ross, J. J. *et al.* Twisted gastrulation is a conserved extracellular BMP antagonist. *Nature*
339 **410**, 479-483, doi:10.1038/35068578 (2001).
340 12 Fristrom, D., Wilcox, M. & Fristrom, J. The distribution of PS integrins, laminin A and F-
341 actin during key stages in Drosophila wing development. *Development* **117**, 509-523 (1993).

342 13 Maartens, A. Intercellular signalling, cell fate and cell shpae in the Drosophila pupal wing.
343 *Doctoral thesis (DPhil), University of Sussex* (2012).
344 14 Martin, A. C. & Goldstein, B. Apical constriction: themes and variations on a cellular
345 mechanism driving morphogenesis. *Development* **141**, 1987-1998, doi:10.1242/dev.102228
346 (2014).
347 15 Daniel, E. *et al.* Coordination of Septate Junctions Assembly and Completion of Cytokinesis
348 in Proliferative Epithelial Tissues. *Curr Biol* **28**, 1380-1391 e1384,
349 doi:10.1016/j.cub.2018.03.034 (2018).
350 16 Lee, T. & Luo, L. Mosaic analysis with a repressible cell marker for studies of gene function
351 in neuronal morphogenesis. *Neuron* **22**, 451-461 (1999).
352 17 Shimada, Y., Yonemura, S., Ohkura, H., Strutt, D. & Uemura, T. Polarized transport of
353 Frizzled along the planar microtubule arrays in Drosophila wing epithelium. *Dev Cell* **10**,
354 209-222, doi:10.1016/j.devcel.2005.11.016 (2006).
355 18 Franke, J. D., Montague, R. A. & Kiehart, D. P. Nonmuscle myosin II generates forces that
356 transmit tension and drive contraction in multiple tissues during dorsal closure. *Curr Biol*
357 **15**, 2208-2221, doi:10.1016/j.cub.2005.11.064 (2005).
358 19 Mitonaka, T., Muramatsu, Y., Sugiyama, S., Mizuno, T. & Nishida, Y. Essential roles of
359 myosin phosphatase in the maintenance of epithelial cell integrity of Drosophila imaginal
360 disc cells. *Dev Biol* **309**, 78-86, doi:10.1016/j.ydbio.2007.06.021 (2007).
361 20 Entchev, E. V., Schwabedissen, A. & Gonzalez-Gaitan, M. Gradient formation of the TGF-
362 beta homolog Dpp. *Cell* **103**, 981-991 (2000).
363 21 Adachi-Yamada, T. & O'Connor, M. B. Morphogenetic apoptosis: a mechanism for
364 correcting discontinuities in morphogen gradients. *Dev Biol* **251**, 74-90 (2002).

365 22 Moreno, E., Basler, K. & Morata, G. Cells compete for decapentaplegic survival factor to
366 prevent apoptosis in Drosophila wing development. *Nature* **416**, 755-759,
367 doi:10.1038/416755a (2002).
368 23 Moreno, E. & Basler, K. dMyc transforms cells into super-competitors. *Cell* **117**, 117-129,
369 doi:10.1016/s0092-8674(04)00262-4 (2004).
370 24 Affolter, M. & Basler, K. The Decapentaplegic morphogen gradient: from pattern formation
371 to growth regulation. *Nat Rev Genet* **8**, 663-674, doi:10.1038/nrg2166 (2007).
372 25 Restrepo, S., Zartman, J. J. & Basler, K. Coordination of patterning and growth by the
373 morphogen DPP. *Curr Biol* **24**, R245-255, doi:10.1016/j.cub.2014.01.055 (2014).
374 26 Bowling, S., Lawlor, K. & Rodriguez, T. A. Cell competition: the winners and losers of
375 fitness selection. *Development* **146**, doi:10.1242/dev.167486 (2019).
376 27 Gui, J. *et al.* Coupling between dynamic 3D tissue architecture and BMP morphogen
377 signaling during Drosophila wing morphogenesis. *Proc Natl Acad Sci U S A* **116**, 4352-
378 4361, doi:10.1073/pnas.1815427116 (2019).
379 28 Milan, M., Campuzano, S. & Garcia-Bellido, A. Cell cycling and patterned cell proliferation
380 in the Drosophila wing during metamorphosis. *Proc Natl Acad Sci U S A* **93**, 11687-11692
381 (1996).
382 29 Gui, J. *et al.* Coupling between dynamic 3D tissue architecture and BMP morphogen
383 signaling during Drosophila wing morphogenesis. *Proc Natl Acad Sci U S A*,
384 doi:10.1073/pnas.1815427116 (2019).
385 30 Sivakumar, A. & Kurpios, N. A. Transcriptional regulation of cell shape during organ
386 morphogenesis. *J Cell Biol* **217**, 2987-3005, doi:10.1083/jcb.201612115 (2018).
387 31 Heer, N. C. & Martin, A. C. Tension, contraction and tissue morphogenesis. *Development*
388 **144**, 4249-4260, doi:10.1242/dev.151282 (2017).

389 32 Tracy Cai, X. *et al.* AWD regulates timed activation of BMP signaling in intestinal stem
390 cells to maintain tissue homeostasis. *Nat Commun* **10**, 2988, doi:10.1038/s41467-019-
391 10926-2 (2019).
392 33 Fereres, S., Hatori, R., Hatori, M. & Kornberg, T. B. Cytoneme-mediated signaling essential
393 for tumorigenesis. *PLoS Genet* **15**, e1008415, doi:10.1371/journal.pgen.1008415 (2019).
394 34 Rauzi, M., Lenne, P. F. & Lecuit, T. Planar polarized actomyosin contractile flows control
395 epithelial junction remodelling. *Nature* **468**, 1110-1114, doi:10.1038/nature09566 (2010).
396 35 Ashburner, M., Golic, K. G. & Hawley, R. S. Drosophila: A Laboratory Handbook, Second
397 Edition (Cold Sprig Habor, NY: Cold Spring Habor Press). (2004).
398 36 Schindelin, J. *et al.* Fiji: an open-source platform for biological-image analysis. *Nat*
399 *Methods* **9**, 676-682, doi:10.1038/nmeth.2019 (2012).
400 37 Ferreira, T. *et al.* tferr/Scripts: BAR 1.5.1. *Zenodo* **doi:10.5281/zenodo.495245** (2017).
401 38 Ollion, J., Cochennec, J., Loll, F., Escude, C. & Boudier, T. TANGO: a generic tool for
402 high-throughput 3D image analysis for studying nuclear organization. *Bioinformatics* **29**,
403 1840-1841, doi:10.1093/bioinformatics/btt276 (2013).

404

405 **Materials and methods**

406 **Fly genetics**

407 *UAS-mCD8::GFP* (#5137), *en-Gal4* (#30564), shi^{ts1} (#7068) and UAS-MBS.N300 (#63791) were
408 obtained from the Bloomington *Drosophila* Stock Centre. $UAS\text{-}tkv^{Q253D}$ and cv^{70} were described
409 previously[8,10]. *E-cad::GFP* was obtained from H. Ohkura[17], *MyoII::RFP* from R. Le Borgne[15],
410 *UAS-MyoII-DN* from D. Kiehart[18], *Tkv::V5* from G. Pyrowolakis[32], *Dpp::mCherry* from T.
411 Kornberg[33] and *sqh-GAP43::mCherry* from A. Martin[34]. Populations of mixed sex were used except
412 for when using *yw* or $tubP\text{-}Gal80^{ts}$ on X, where females were selected, and experiments involving
413 *crossveinless*, where only males were used. The ages of pupal wings at dissection are given at

414 developmental timepoints equivalent to 25˚C. Calculations for relative developmental timing at
415 18˚C, 25˚C and 29˚C were based on previously published data and rounded to the nearest hour[35].
416 For experiments using *en-Gal4*, pupae were raised at 18°C for 22 hours after pupariation, and then
417 shifted to 29°C for either 10 (Fig. 3b, c, d, e, Supplementary Fig. 2a, 4d) or 12 (Supplementary Fig.
418 4b-c) hours before dissection and fixation. The exception to this was the experiment involving
419 UAS-MBS.N300, when pupae were raised at 29˚C for 21 hours after pupariation (Supplementary
420 Fig. 2b). For clone generation, larvae were raised at 25°C for 3-4 days AEL (or 18°C for 6-7 days
421 AEL), before being heat shocked in a 37°C water bath for 1 hour. Vials containing larvae were then
422 either placed at 18°C until at the white pre-pupal stage, and then transferred to 29°C for 21 hours
423 before dissection and fixation (Fig. 3g, i, Supplementary Figs 1b, 2d, e) or transferred to 25°C for
424 20 hours after pupariation and then 34°C for 3hours (Fig. 3j, Supplementary Fig. 3). For time-lapse
425 imaging, pupae were raised at 25°C until 17 hours after the pre-pupal stage. They were then moved
426 to room temperature for one hour, during which windows were cut into the pupal case and pupae
427 mounted, before being imaged as previously described[29].
428
429 **Full genotypes**
430 Fig. 1d-e, Fig. 4 and Supplementary Fig. 4a : *yw*
431 Fig. 1f: *yw; ubi-E-cad::GFP,* or *cv^{70}; ubi-E-cad::GFP*
432 Fig. 1g and Supplementary Fig. 1a: *MyoII::RFP,* or *MyoII::RFP, cv^{70}*
433 Fig. 2 and Supplementary videos 1-3: *ubi-E-cad::GFP/sqh-Gap43::mCherry*
434 Fig. 3e-f and Supplementary Fig. 4d: *en-Gal4/UAS-mCD8::GFP; tubP-Gal80^{ts},* or *en-Gal4/UAS-*
435 *MyoII-DN; tubP-Gal80^{ts}*
436 Fig. 3g and Supplementary Fig. 2d, e: *hs-Flp; tubP-Gal4 UAS-mCD8::GFP/UAS-MyoII-DN; tubP-*
437 *Gal80 FRT^{82B} /FRT^{82B}*
438 Fig 3i: *hs-Flp FRT^{82B}; tubP-Gal4 UAS-mCD8::GFP/UAS-tkv^{Q253D}; FRT^{82B} tubP-Gal80/FRT^{82B}*

439 Fig 3j: *hs-Flp, tubP-Gal80, FRT^{19A}/shi^{ts1}, FRT^{19A}; tubP-Gal4, UAS-mCD8::GFP/UAS-tkv^{Q253D}*

440 Fig 5 and Supplementary Fig 5a: *yw; tkv-V5/CyO*

441 Supplementary Fig. 1b: *hs-Flp/tubP-Gal80^{ts}, MyoII::RFP; tubP-Gal4 UAS-mCD8::GFP/UAS-*

442 *tkv^{Q253D}; tubP-Gal80 FRT^{82B} /FRT^{82B}*

443 Supplementary Fig. 2a: *cv^{70}; en-Gal4/+; tubP-Gal80^{ts}*, or *cv^{70}; en-Gal4/UAS-MyoII-DN; tubP-*

444 *Gal80^{ts}*

445 Supplementary Fig. 2b, c: *en-Gal4/+; UAS- mbs.N300/tubP-Gal80^{ts} or en-Gal4/UAS-mCD8::GFP;*

446 *tubP-Gal80^{ts}*

447 Supplementary Fig. 3: *hs-Flp, tubP-Gal80, FRT^{19A}/Shi^{ts1}, FRT^{19A}; TubP-Gal4, UAS-mCD8::GFP*

448 Supplementary Fig. 4b-c: *en-Gal4/sqh-Gap43::mCherry; tubP-Gal80^{ts}*, or *en-Gal4/UAS-MyoII-DN,*

449 *sqh-Gap43::mCherry; tubP-Gal80^{ts}*

450 Supplementary Fig. 5b: *dpp::mCherry* (II)

451

452 **Immunohistochemistry**

453 Pupae were fixed in 3.7% formaldehyde (Sigma-Aldrich) for two nights at 4°C before dissecting the

454 pupal wings and blocking with Normal Goat Serum (10%) overnight. Both primary and secondary

455 antibody incubations also took place overnight at 4°C. The following primary antibodies were used:

456 mouse anti-DLG1 [1:40; Developmental Studies Hybridoma Bank (DSHB), University of Iowa]

457 and rabbit anti-phospho-SMAD1/5 (1:200; Cell Signaling Technologies) mouse anti-V5 (1:200,

458 Invitrogen). Secondary antibodies were anti-rabbit IgG Alexa 568 (1:200, Invitrogen), anti-mouse

459 IgG Alexa 647 (1:200; Life technologies), anti-rabbit IgG Alexa 647 (1:200; Life technologies). F-

460 actin was stained with Alexa 488 conjugated phalloidin (1:200; Life technologies).

461

462 **Imaging and Image Analysis**

463 Confocal images and time-lapse images were acquired using a Leica SP8 STED confocal
464 microscope. Time-lapse images were processed using Imaris v9.1.2 (Bitplane/Oxford Instruments)
465 and snapshots segmented by hand in Image J/Fiji (v. 1.52p and 1.53c)[36]. All other images were
466 processed and analysed using Fiji. All images (with the exception of cross sections), including time-
467 lapse snap shots, are maximum composites. A median filter was applied to pMad images, and
468 median and minimum filters were applied to Tkv::V5 images in Fiji. The heatmaps were generated
469 using the ROI color coder plugin, part of the BAR collection of ImageJ[37].
470 The number of pMad-positive cells within the PCV field was calculated by first excluding adjacent
471 LV nuclei by marking the predicted trajectory of the LV–PCV boundary by drawing across from
472 the edge of L4 and L5 on either side of the PCV. pMad positive nuclei between these lines were
473 then counted. Z projections of median filtered images were used for quantification, using the stacks
474 for reference.
475 The apical and basal sizes of field cells were analysed using individual slices of stacks in Fiji. Cells
476 that showed pMad staining in the nucleus were traced and measured. The most apical or basal slice
477 where the cell outline was clear was used for each cell. Cells at the centre and posterior portion of
478 the PCV were analysed. Cells in the middle 50% of the PCV (as indicated by pMad) were
479 designated central cells and those outside this peripheral.
480 Cell volumes were determined for the same cells for which apical and basal surface areas had been
481 measured. To measure cell volumes, the RoiManager3D tool was used, a plug-in in the 3D ImageJ
482 Suite (version 3.96)[38]. In any z-sections for which cell boundaries were ambiguous, the boundaries
483 were drawn as best-guess interpolations between the segmented boundaries of neighboring apical
484 and basal z-sections. Cells with more than one consecutive ambiguous z-section boundary were
485 excluded from the subsequent volume determinations.

486 Figure 1g and Supplementary Fig 1a were generated from the same stacks. Figure 4 and
487 Supplementary Figure 4a represent analyses of the same data set, as do Figure 3b-e and
488 Supplementary Figure 4d, and Figure 5 and Supplementary Figure 5a, respectively.
489 All representative images are representative of at least three biological replicates.
490
491 **Statistics**
492 Statistical analyses were performed using GraphPad Prism software (v.8.3.0, GraphPad). The
493 number for all quantified data is indicated in the figure legends. All *P* values were calculated using
494 a two-sided Mann-Whitney test and specified in the figure legends and in the corresponding plots.
495

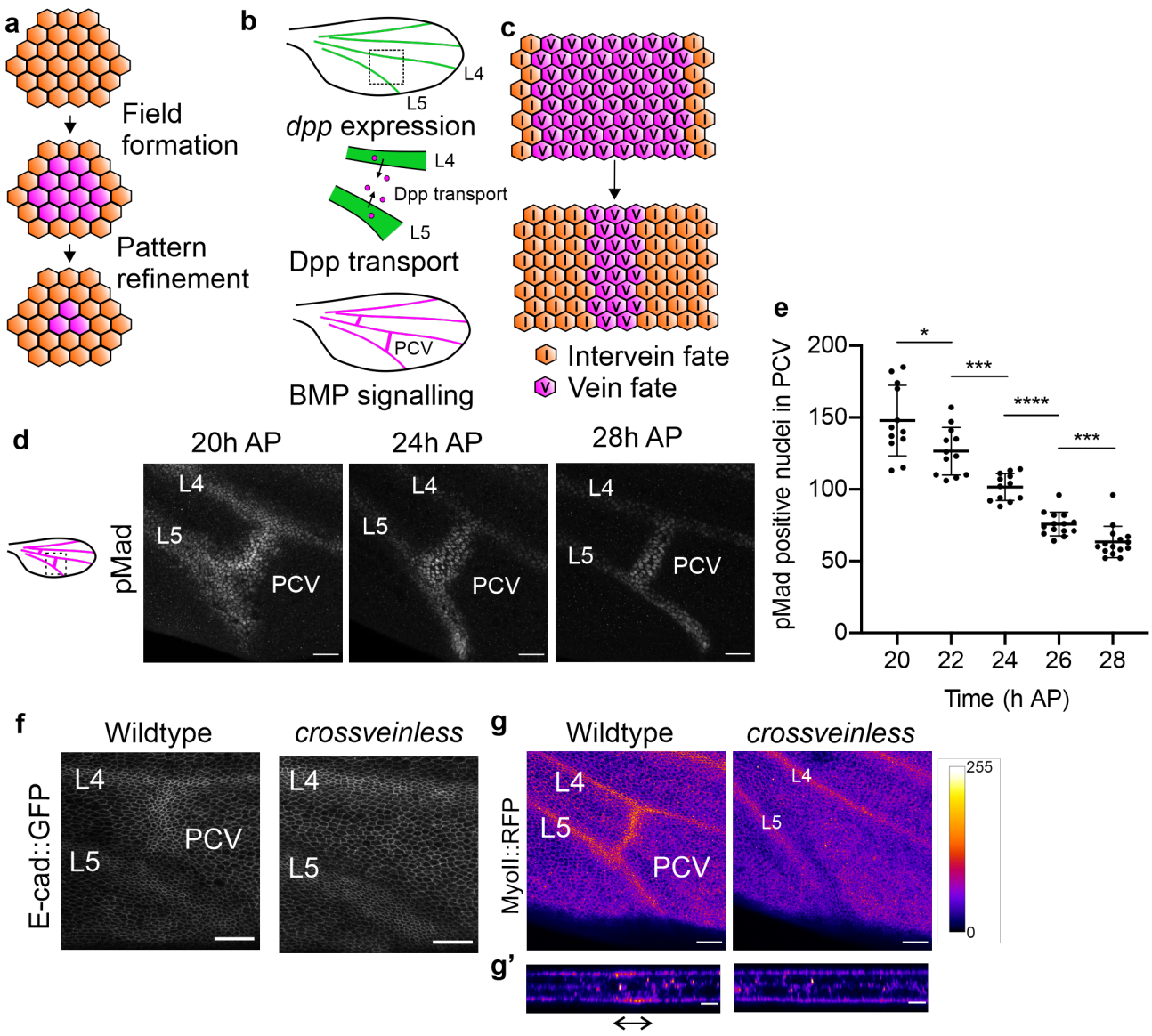

Fig. 1: The PCV field refines during vein patterning and morphogenesis. a, Schematic depicting the refinement of developmental patterns from an initial field to cells committing to a fate. **b,** The expression pattern and signalling pattern of the BMP ligand Dpp in the developing pupal wing. L4, L5, and PCV denote longitudinal veins 4, 5, and posterior crossvein, respectively. Top: *dpp* mRNA (green) is expressed in longitudinal veins, but not in crossveins during early pupal stages. Middle: Schematic model of Dpp/BMP ligand transport from the longitudinal veins into PCV. Bottom: BMP signalling (magenta) is detected at all wing vein primordia including longitudinal veins and crossveins. **c,** Schematic depicting the refinement of the BMP signalling pattern in the PCV field. **d,** BMP signalling (shown by pMad) in the PCV field of wild type pupal

506 wings at 20 h, 24 h and 28 h AP. Left: Schematic of pupal wing. Approximate position of imaging
507 is shown as a square. Median filter applied. **e,** The number of cells in which BMP signalling is
508 occurring during the refinement period. Sample sizes are 12 (20 h), 12 (22 h), 12 (24 h), 14 (26 h)
509 and 15 (28 h). *P = 0.0252, 22-24h: ***P = 0.0005, ****P < 0.0001, 26-28h: ***P = 0.0002. Data
510 are mean ± s.d. and were analysed by two-sided Mann-Whitney test. **f,** E-cad::GFP in the PCV
511 region in wild type (left) and *crossveinless* mutant (right) pupal wings at 24 h AP. Apical cell
512 shapes are highlighted by max composite of E-cad:GFP. **g,** Heatmap of the apical intensity of
513 MyoII::RFP in cells of the PCV region in wildtype (left) and *crossveinless* mutant (right) pupal
514 wings at 24h AP. Optical cross sections on the PCV region are shown at the lower panel (**g'**).
515 Prospective PCV position is indicated by double-headed arrow. The apical distribution of MyoII is
516 shown through the PCV region. Scale bars: 25 μm for **d**, **f** and **g,** and 10 μm for **g'**.
517

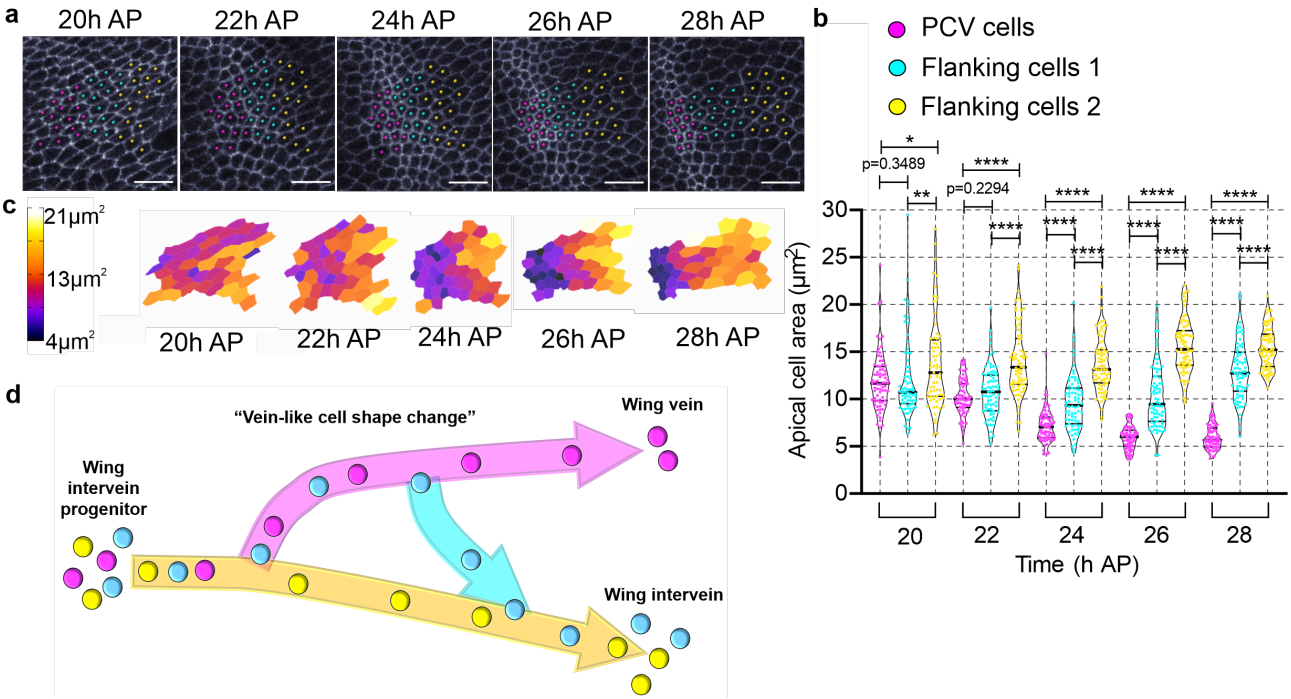

Fig. 2: Changes in cell shape are dynamic and transient during pattern refinement. a, Time-lapse images of E-cad::GFP in the PCV region at 20 h, 22 h, 24 h, 26 h and 28 h AP. Three clusters of cells are marked. Future PCV cells (magenta) show progressive apical constriction. Cells immediately adjacent to future PCV cells (cyan) show transient apical constriction during 22 h and 26 h AP before reverting to an intervein-like structure. Cells further from future PCV cells (yellow) do not show apical constriction. PCV cells are categorised by their shape at 28 h AP and flanking categories by their relative position and shape at 28 h AP. Scale bars: 10 µm. **b,** Apical size of PCV cells and their neighbours during the refinement period. N=75 cells per category (15 cells tracked per category in each wing, for 5 wings). Violin plots show median, and 25th and 75th percentiles. Data from five independent time-lapse images. Each data point [PCV cells: magenta, cells adjacent to PCV (Flanking cells 1): cyan, cells further from PCV (Flanking cells 2): yellow] represents one cell. $*P = 0.0185$, $**P = 0.0071$, $****P < 0.0001$. Data were analysed by two-sided Mann-Whitney test. **c,** Heat map showing the changes in apical area of cells of the PCV field. The heatmap was produced using the ROI colour coder plugin, part of the BAR collection of ImageJ. The same cells are shown as in 2a. **d,** Schematic of changes in fate path during PCV patterning. Cells that are

initially on a vein-like cell shape (cyan) lose competence during patterning, and move outside of the vein fate path (magenta) into the intervein fate path (yellow).

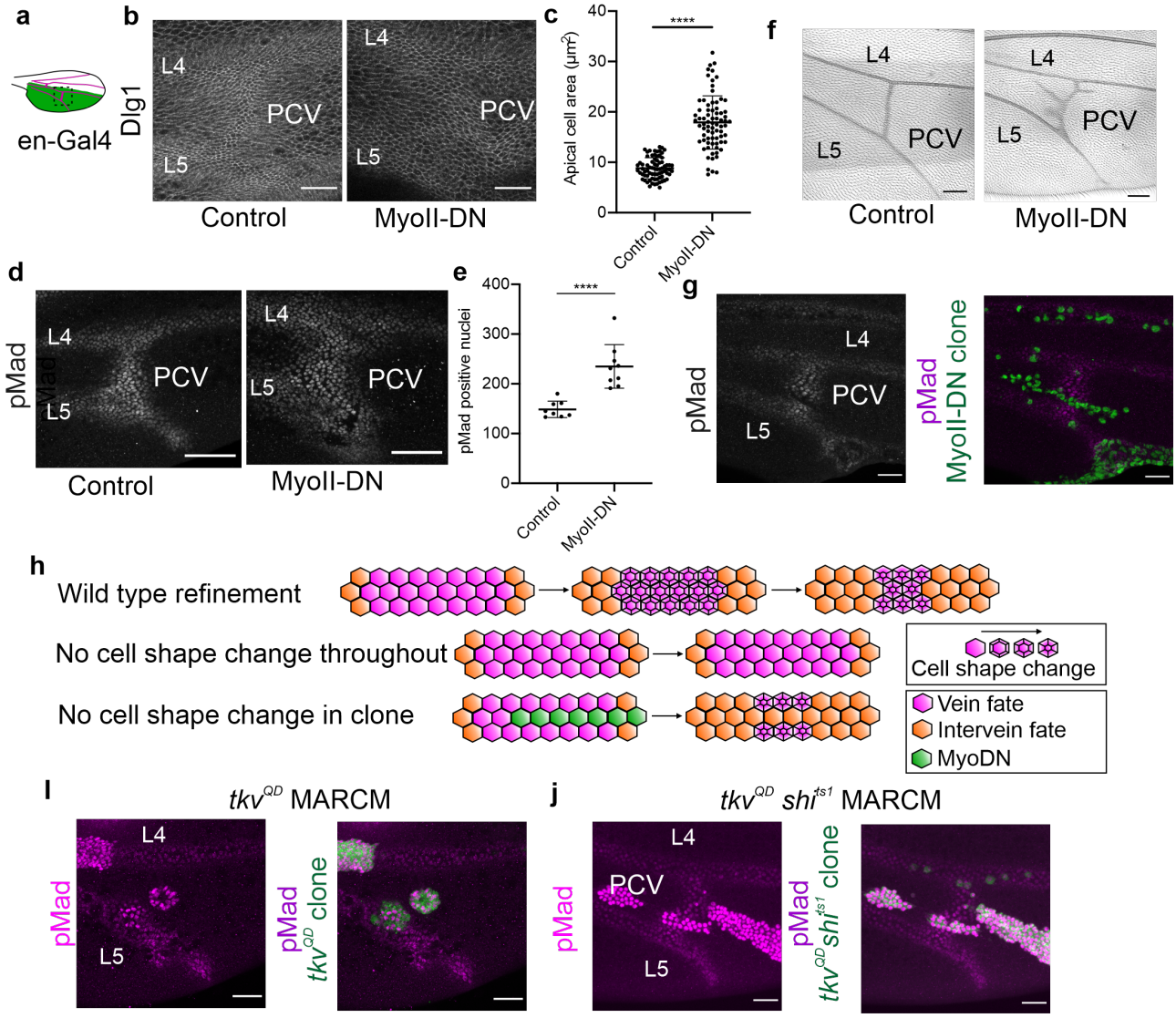

537

538 **Fig. 3: Loss of MyoII activity has context-specific effects on BMP signalling pattern**

539 **refinement. a,** Schematic of pupal wing. Posterior region of the wing and Engrailed-Gal4

540 expression pattern is shown in green. Approximate position of imaging is shown as a square (dotted

541 outline). **b,** Apical cell shape (Dlg1) in the PCV region in control (left, *en* > *mCD8::GFP*) and

542 MyoII attenuated pupal wings (right, *en* > *MyoII-DN*) at 23 h AP. **c,** Apical size of cells in which

543 BMP signalling is occurring (and thus are within the PCV field) in the PCV of 23h AP pupal wings.

544 N=75 cells per category (15 cells in each wing, for 5 wings). ****$P < 0.0001$. Data are mean ± s.d.

545 and were analysed by two-sided Mann-Whitney test. **d,** pMad expression in the PCV region in

546 control (left, *en* > *mCD8::GFP*) and MyoII attenuated pupal wings (right, *en* > *MyoII-DN*) at 23 h

547 AP. MyoII-DN was expressed throughout the posterior wing by *en-Gal4* for 10 hours prior to

548 dissection. Median filter applied. **e,** Number of cells in which BMP signalling is occurring (and thus
549 are within the PCV field) in the PCV of 23h AP pupal wings. N = 8 (control) and 9 (MyoII-DN)**.**
550 ****$P < 0.0001$. Data are mean ± s.d. and were analysed by two-sided Mann-Whitney test. **f,** Adult
551 wings in the PCV region in control (left, *en > mCD8::GFP*) and MyoII attenuated pupal wings
552 (right, *en > MyoII-DN*). **g,** Effects of clonal expression of MyoII-DN within a subset of cells of the
553 PCV field. pMad staining alone (white, left), or pMad staining (magenta), MyoII-DN expressing
554 clones (green) at 25 h AP (right). Median filter applied to pMad staining. **h,** Top: Schematic
555 depicting model of wild type pattern refinement whereby loss of cell shape changes from cells at the
556 edge of the PCV field results in their exclusion from the field (by loss of BMP signalling and thus
557 cell fate). Middle: Loss of MyoII activity and cell shape change throughout the PCV blocks
558 refinement**.** Bottom: Loss of MyoII activity in a subset of PCV cells can lead to loss of signal and
559 fate (ectopic refinement). **i,** Effects of clonal expression of Tkv^{QD} within a subset of cells of the
560 PCV field. pMad staining alone (magenta, left), or pMad staining (magenta) Tkv^{QD}-expressing
561 clones (green) at 25 h AP (right). Median filter applied to pMad staining. **j,** Effects of Tkv^{QD} in
562 shi^{ts1} clones within a subset of cells of the PCV field. pMad staining alone (magenta, left), or pMad
563 staining (magenta) shi^{ts1} clones expressing Tkv^{QD} (green) at 24 h AP (right). Median filter applied
564 to pMad staining. Scale bars: 50 µm for **b, d, f, i, j** and 25 µm for **g**.
565

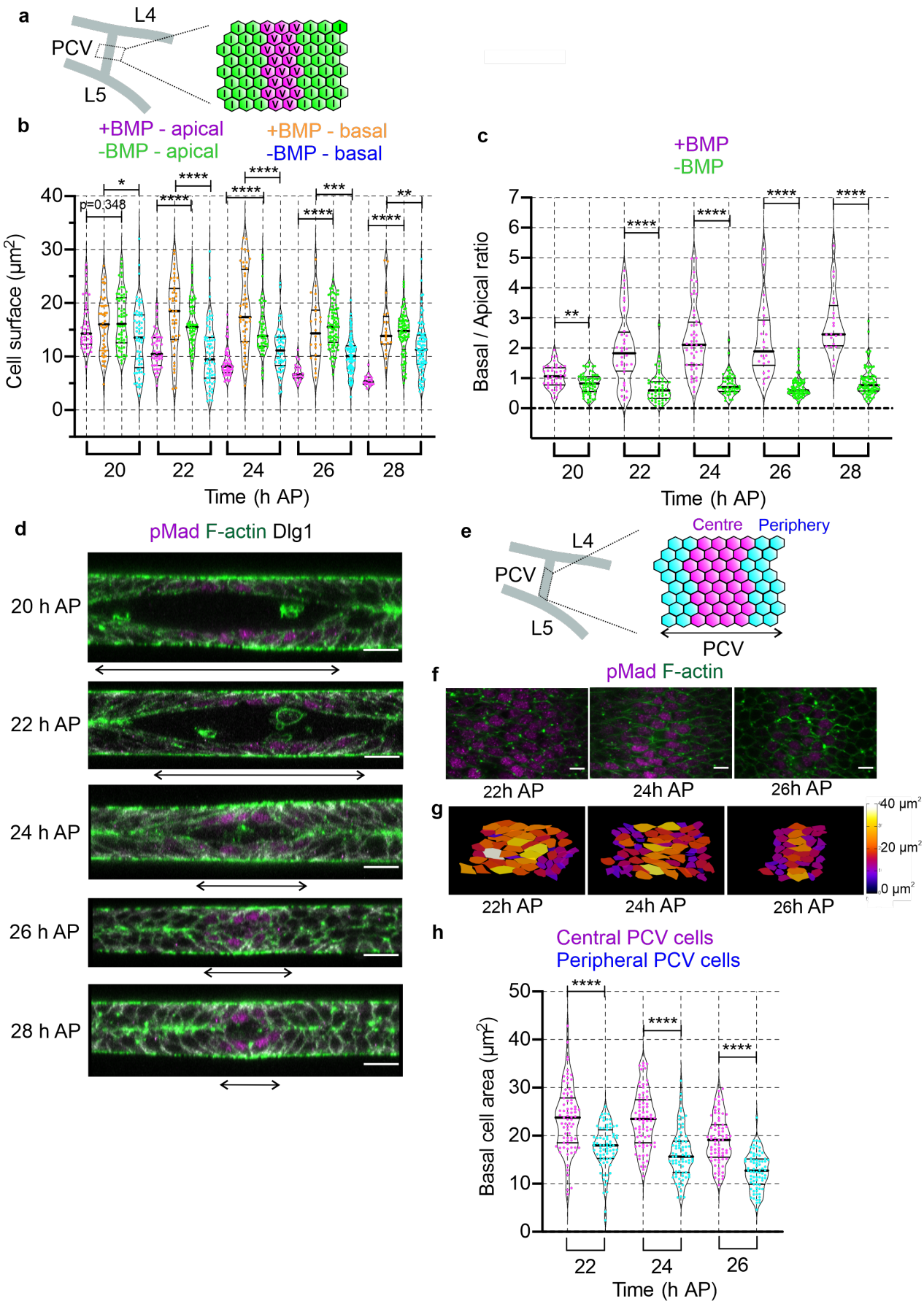
a
L4
PCV
L5
b
+BMP - apical
-BMP - apical
+BMP - basal
-BMP - basal
Cell surface (µm²)
p=0.348
Time (h AP)
c
+BMP
-BMP
Basal / Apical ratio
Time (h AP)
d
pMad F-actin Dlg1
20 h AP
22 h AP
24 h AP
26 h AP
28 h AP
e
L4
PCV
L5
Centre
Periphery
PCV
f
pMad F-actin
22h AP
24h AP
26h AP
g
40 µm²
20 µm²
0 µm²
22h AP
24h AP
26h AP
h
Central PCV cells
Peripheral PCV cells
Basal cell area (µm²)
Time (h AP)

566

567 **Fig. 4: BMP signal induces apical constriction and basal expansion in the PCV field during**
568 **PCV morphogenesis. a,** Schematic of PCV field. Approximate position of cell area within and
569 outside of the PCV field is shown as a square (left). Schematic of cells within (magenta) and outside
570 of (green) PCV field during the refinement period. **b,** Apical and basal surface areas of cells within
571 and outside of the PCV field during the refinement period. Sample sizes (from 5 wings) are 40 (20 h
572 +BMP), 60 (20 h –BMP), 40 (22 h +BMP), 60 (22 h –BMP), 44 (24 h +BMP), 48 (24 h –BMP), 22
573 (26 h +BMP), 80 (24 h –BMP), 20 (28 h +BMP) and 79 (28 h –BMP). Violin plots show median,
574 and 25th and 75th percentiles. Data from five independent images. Each data point [cells within the
575 PCV: apical (magenta) and basal (orange); cells outside of the PCV: apical (green) and basal
576 (cyan)] represents one cell. $*P = 0.0329$, $**P = 0.0037$, $***P = 0.0002$, $****P < 0.0001$. Data were
577 analysed by two-sided Mann-Whitney test. **c,** Ratio of basal and apical surface of cells in **b**. Each
578 data point [cells within the PCV (magenta) and cells outside of the PCV (green)] represents one
579 cell. $**P = 0.0030$, $****P < 0.0001$. **d,** Optical cross sections focused on the PCV regions showing
580 pMad (magenta) Dlg1 (white) and F-actin (green) at 20 h, 22 h, 24 h, 26 h and 28 h AP. Prospective
581 PCV positions are indicated by double-headed arrows. **e,** Schematic of PCV field. Approximate
582 position of cell area within the PCV field is shown as a square (left). Schematic of cells both central
583 (magenta) and peripheral (cyan) PCV field during the refinement period. **f,** Max composites
584 showing basal cell shape of PCV field cells at the level of central PCV cell basal surface during the
585 refinement period. pMad staining (magenta) and F-actin (green) at 22h, 24h and 26h AP (left).
586 Median filter applied to pMad staining. **g**, Heat map showing the changes in basal area of cells of
587 the PCV field. The heatmap was produced using the ROI colour coder plugin, part of the BAR
588 collection of ImageJ. **h,** Basal cell areas of peripheral and central PCV cells during refinement. N =
589 75 (15 cells per wing, data from 5 wings pooled). Violin plots show median, and 25th and 75th
590 percentiles. Each data point (central PCV cells: magenta, peripheral PCV cells: cyan) represents one

591 cell. ****$P < 0.0001$. Data were analysed by two-sided Mann-Whitney test. The same wings are

592 analysed for all of Figure 4. Scale bars: 10 μm for **d** and 5 μm for **f.**

593

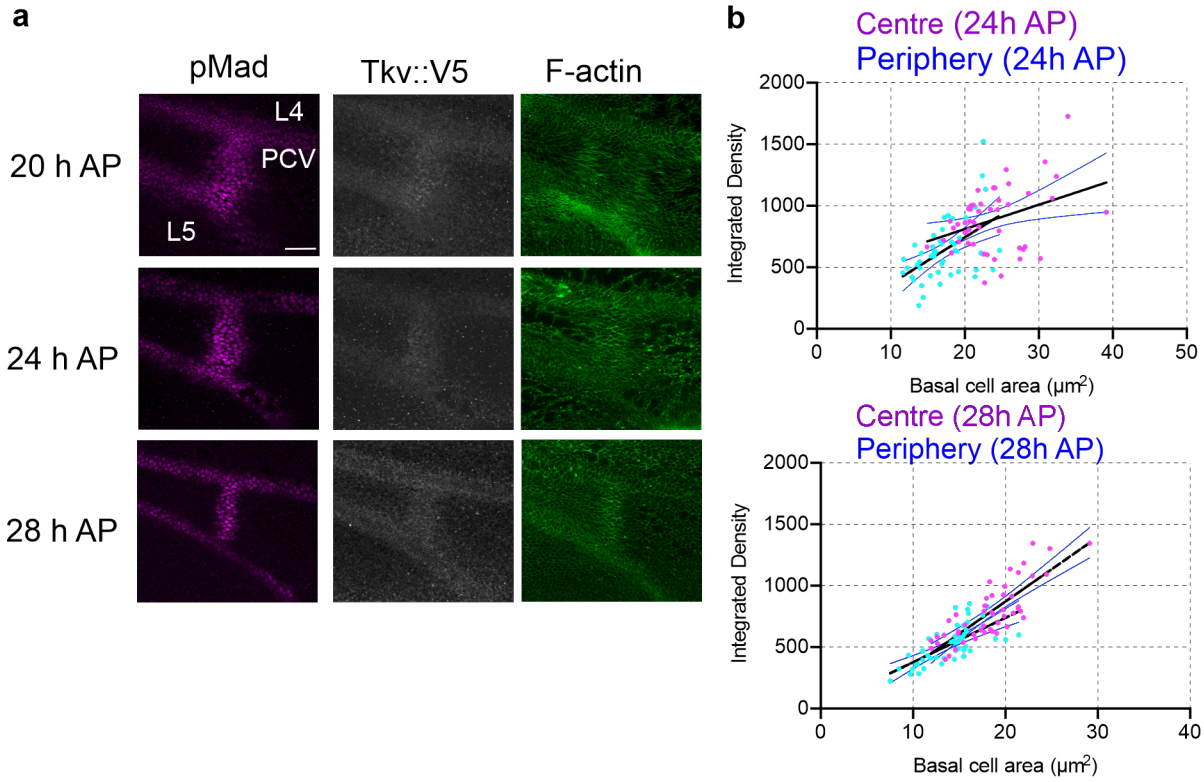

Fig. 5: BMP receptor Tkv is basally localized in the PCV cells to sustain competence for BMP signalling. a, Tkv is localized at basal compartment in the PCV region during the refinement period. pMad expression (left, magenta), Tkv::V5 (middle, white) and F-actin (right, green) in the PCV region at 20 h, 24 h and 28 h AP. Median filter applied to pMad and, median and minimum filter applied to Tkv::V5. Images are maximum composites of basal region. Scale bar: 25 µm. **b,** Comparison of the integrated density of Tkv::V5 staining in the basal compartment and basal cell areas of peripheral and central PCV cells at 24 h and 28 h AP. Each data point (central PCV cells: magenta, peripheral PCV cells: cyan) represents one cell. N = 50 (10 cells per wing, data from 5 wings pooled). Black lines indicate mean levels and blue lines indicate error with 95% confidence intervals.

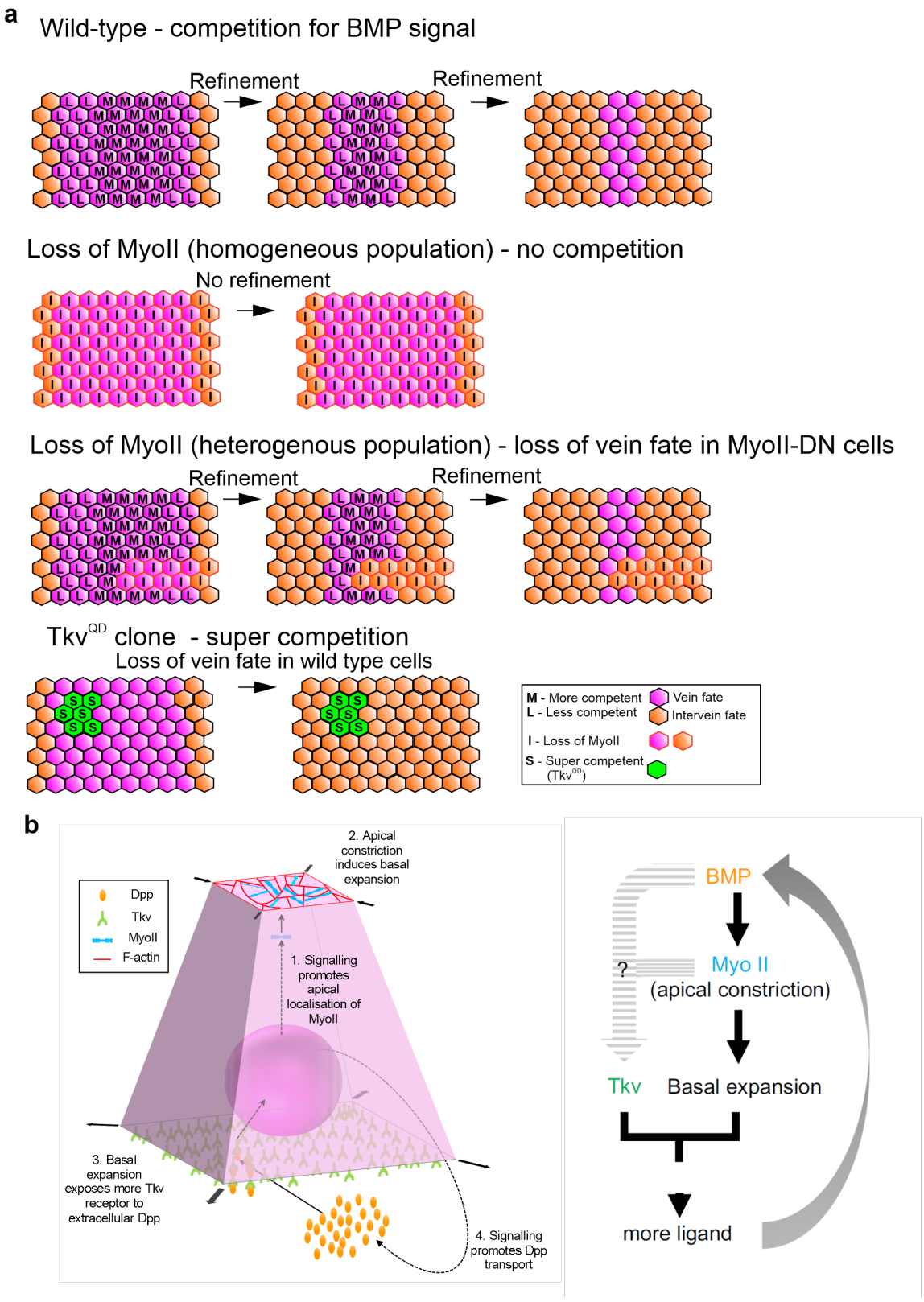

606

607 **Fig. 6: Schematic showing a mechano-chemical feedback loop in the PCV cells during**

608 **refinement period. a,** Schematics of competition for BMP signal during PCV development. Top:

609 Schematic depicting model of wild type pattern refinement whereby loss of cell shape changes from

610 cells at the edge of the PCV field results in the their exclusion from the field (by loss of BMP
611 signalling and thus cell fate). Second row: Loss of MyoII activity and cell shape change throughout
612 the PCV blocks refinement as no competition occurs. Third row: Loss of MyoII activity in a subset
613 of PCV cells can lead to loss of signal and fate (ectopic refinement). Bottom: Clones expressing
614 Tkv^{QD} lose BMP signalling in the PCV region in a non-autonomous manner, resulting in loss of
615 PCV cell fate. **b,** Mechano-chemical feedback loop. 1. BMP signal promotes apical constriction
616 through induction of apical Myosin II. 2. Apical Myosin II activity induces basal expansion. 3.
617 Basal expansion exposes more basally localized Tkv receptors to extracellular Dpp. 4. Promoting
618 BMP signal, feeding back into further shape change and promoting Dpp transport to the cell.
619
620